V Conferência Nacional de Mecânica dos Fluidos, Termodinâmica e Energia
MEFTE 2014, 11–12 Setembro 2014, Porto, Portugal

Improvement of the energy distribution in isotropic turbulent viscoelastic fluid models

P. R. Resende[1], F. T. Pinho[2], P. J. Oliveira[3]

[1]Grupo de Automação e Sistemas Integráveis, UNESP - Univ. Estadual Paulista, 18087-180, Sorocaba - SP, Brazil
[2]Centro de Estudos de Fenómenos de Transporte, Departamento de Engenharia Mecânica, Faculdade de Engenharia Universidade do Porto, Rua Dr. Roberto Frias s/n, 4200-465 Porto, Portugal
[3]Departamento de Engenharia Electromecânica, Universidade da Beira Interior, Rua Marques D'Avila e Bolama, 6201-001 Covilhã, Portugal
email: resende@sorocaba.unesp.br, fpinho@fe.up.pt, pjpo@ubi.pt

ABSTRACT: Strong anisotropy effects in turbulent viscoelastic fluids flows limits the use of isotropic turbulent closures, for example the *k-ε* and *k-ω* turbulent model types. Existing viscoelastic models based on the Boussinesq hypothesis fail to predict correctly the turbulent kinetic energy behaviour for the various drag reduction (DR) regimes, and in particular at high drag reduction. To address this limitation and in particular to improve the near-wall distribution of the turbulent kinetic energy (TKE) a different closure, based on the fluid relaxation time, has been developed for the Reynolds stress tensor. With the new model the TKE is better predicted close to the wall, where the viscoelastic fluids have more impact, and this improves also the TKE distribution away from the wall. The different contributions to the transport equation of TKE are analyzed, showing the impact of the new model, and the effect of drag reduction increase on the distribution is investigated in detail.

KEY-WORDS: Viscoelastic fluids; Turbulence; Isotropic models; Energy distribution.

1 INTRODUCTION

The increased availability of powerful computational resources has fostered research on Direct Numeric Simulation (DNS) of viscoelastic pipe and channel flows, [1-4]. This has allowed an increased understanding of turbulence of viscoelastic solutions as well as the analysis of time-averaged quantities of the governing equations that have helped the development of adequate turbulence closures for the various drag reduction regimes.

The first viscoelastic turbulence models developed for viscoelastic fluids following this type of approach were by Pinho et al. [5] and Resende et al. [6]. They relied on several viscoelastic closures in the context of isotropic turbulent models leading originally to a *k-ε* type turbulence model. Those models were able to capture with good accuracy the flow characteristics in the low and intermediate regimes of DR, but the Boussinesq hypothesis becomes increasingly difficult to justify as DR increases because of the increasingly strong turbulence anisotropy. Hence, the previous models were not able to predict correctly the turbulent kinetic energy at high drag reductions and for this reason a new model for the Reynolds stress tensor is here developed that attempts to address those limitations. In section 2 the governing equations and model are presented, its performance is discussed in section 3 and the conclusions summarize the main findings.

2 GOVERNING EQUATIONS

The governing equations for turbulent flows of viscoelastic fluids using the Finitely Extensive Nonlinear Elastic constitutive equation with the Peterlin approximation (FENE-P) in the context of Reynolds-averaged quantities are the Reynolds-averaged continuity equation, momentum equation and a Reynolds-averaged evolution equation for the conformation tensor together with an expression relating the conformation tensor with the polymer stress tensor. The momentum equation is giving by

$$\rho\frac{\partial U_i}{\partial t}+\rho U_k\frac{\partial U_i}{\partial x_k}=-\frac{\partial \overline{p}}{\partial x_i}+\eta_s\frac{\partial^2 U_i}{\partial x_k\partial x_k}-\frac{\partial}{\partial x_k}\left(\rho\overline{u_i u_k}\right)+\frac{\partial \overline{\tau}_{ik,p}}{\partial x_k} \tag{1}$$

where U is the mean velocity, $\overline{p}$ is the mean pressure, ρ is the fluid density, η_s is the solvent viscosity, $\overline{\tau}_{ik,p}$ is the Reynolds-averaged polymer stress and $-\rho\overline{u_i u_k}$ is the Reynolds stress tensor. Uppercase letters and overbars denote Reynolds-averaged quantities, whereas lowercase letters and primes denote fluctuations.

The Reynolds-averaged polymer stress $\overline{\tau}_{ij,p}$ is based on the FENE-P model and is defined by the following equation

$$\overline{\tau}_{ij,p} = \frac{\eta_p}{\lambda}\left[f\left(C_{kk}\right)C_{ij} - f\left(L\right)\delta_{ij} \right] + \frac{\eta_p}{\lambda}\overline{f\left(C_{kk}+c_{kk}\right)c_{ij}} \tag{2}$$

where η_p and λ are the polymer viscosity coefficient and the relaxation time of the fluid, respectively. The two functions are based on L^2, the maximum dimensionless extensibility of the model dumbbell, and are given by

$$f\left(C_{kk}\right) = \frac{L^2-3}{L^2-C_{kk}} \text{ and } f\left(L\right)=1 \tag{3}$$

The Reynolds-averaged equation describing the evolution of conformation tensor (C_{ij}) is subsequently combined with Eq. (2) to give Eq. (4), where the first-term inside the brackets on the left-hand-side is Oldroyd's upper convective derivative of C_{ij}. The various terms of Eq. (4) have specific designations given below the horizontal brackets.

$$\left[\underbrace{\frac{\partial C_{ij}}{\partial t} + U_k\frac{\partial C_{ij}}{\partial x_k}}_{DC_{ij}/Dt} - \underbrace{\left(C_{jk}\frac{\partial U_i}{\partial x_k} + C_{ik}\frac{\partial U_j}{\partial x_k} \right)}_{M_{ij}} \right] + \underbrace{\overline{u_k\frac{\partial c_{ij}}{\partial x_k}}}_{CT_{ij}} - \underbrace{\left(\overline{c_{kj}\frac{\partial u_i}{\partial x_k}} + \overline{c_{ik}\frac{\partial u_j}{\partial x_k}} \right)}_{NLT_{ij}} = -\frac{\overline{\tau}_{ij,p}}{\eta_p} \tag{4}$$

The NLT_{ij} term is calculated using the closure developed by Resende et al. [6], given by Eq. (5), and the contribution of CT_{ij} is neglected as previously suggested by DNS data analysis, cf. Li et al. [3].

$$\begin{aligned}
NLT_{ij} \equiv{}& \overline{c_{kj}\frac{\partial u_i}{\partial x_k}} + \overline{c_{ik}\frac{\partial u_j}{\partial x_k}} \approx C_{F1}\left[0.055\left(\frac{We_{\tau 0}}{25}\right)^{1.07} + 0.116 \right]\times\frac{C_{ij}\times f(C_{mm})}{\lambda} + \\
&+\frac{\lambda}{f(C_{mm})}\left[C_{F3}\times\left(\frac{25}{We_{\tau 0}}\right)^{0.55}\times\left(\frac{\partial U_j}{\partial x_n}\frac{\partial U_m}{\partial x_k}C_{kn}\frac{\overline{u_i u_m}}{\nu_0\sqrt{2S_{pq}S_{pq}}} + \frac{\partial U_i}{\partial x_n}\frac{\partial U_m}{\partial x_k}C_{kn}\frac{\overline{u_j u_m}}{\nu_0\sqrt{2S_{pq}S_{pq}}} + \right.\right. \\
&\left.\left. + \frac{\partial U_k}{\partial x_n}\frac{\partial U_m}{\partial x_k}\left(C_{jn}\frac{\overline{u_i u_m}}{\nu_0\sqrt{2S_{pq}S_{pq}}} + C_{in}\frac{\overline{u_j u_m}}{\nu_0\sqrt{2S_{pq}S_{pq}}} \right) \right) \right] - \\
&-\frac{\lambda}{f(C_{mm})}\times f_{F1}\times C_{F4}\times\left(\frac{25}{We_{\tau 0}}\right)^{0.55}\times\left[C_{jn}\frac{\partial U_k}{\partial x_n}\frac{\partial U_i}{\partial x_k} + C_{in}\frac{\partial U_k}{\partial x_n}\frac{\partial U_j}{\partial x_k} + C_{kn}\frac{\partial U_j}{\partial x_n}\frac{\partial U_i}{\partial x_k} + C_{kn}\frac{\partial U_i}{\partial x_n}\frac{\partial U_j}{\partial x_k} \right] + \\
&+\frac{\lambda}{f(C_{mm})}\left[\frac{C_{\varepsilon_{F2}}}{We_{\tau 0}}\frac{4}{15}\times\frac{\varepsilon^N}{\left(\nu_s+\nu_{\tau_p}\right)}C_{mm}\times f_{F2}\times\delta_{ij} \right] - C_{F2}We_{\tau 0}{}^{0.74}\left[C_{kj}\frac{\partial U_i}{\partial x_k} + C_{ik}\frac{\partial U_j}{\partial x_k} \right]
\end{aligned} \tag{5}$$

In Eq. (5) $We_{\tau 0}$ is the Weissenberg number, defined as $We_{\tau 0} = \lambda {u_\tau}^2/\nu_0$ based on the friction velociy, u_τ, and on the total zero shear-rate kinematic viscosity, i.e., the sum of the kinematic viscosities of the solvent and polymer, $\nu_0 = \nu_s + \nu_p$, k and ε^N are the turbulent kinetic energy and the rate of dissipation, respectively, and S_{ij} is the rate of deformation tensor, $S_{ij} = \left(\partial U_i/\partial x_j + \partial U_j/\partial x_i\right)/2$.

The Reynolds stress in Eq. (1) is modeled by the Boussinesq hypothesis through the following equation,

$$-\rho\overline{u_i u_j} = 2\rho\left(\nu_T + {\nu_T}^{p*}\right)S_{ij} - \frac{2}{3}\rho k\delta_{ij} \tag{6}$$

where ν_T is the turbulent viscosity and ${\nu_T}^{p*}$ is the extra polymeric turbulent viscosity, respectively. The turbulent viscosity, defined by Eq. (7), was developed by Resende et al. [6] considering both Newtonian and non-Newtonian contributions given in Eqs. (8).

$$\nu_T = {\nu_T}^N - {\nu_T}^P \tag{7}$$

$$\nu_T{}^N = C_\mu \times f_\mu \times \frac{k^2}{\varepsilon^N} \text{ and } \nu_T{}^P = C_\mu{}^P \times f_{DR}{}^p \times \left(\frac{C_{mm}}{L^2}\right)^{0.25} \times \frac{k^2}{\varepsilon^N} \tag{8}$$

The closures for the turbulent viscosities involve the damping function f_μ defined by $f_\mu = \left[1-\exp\left(-y^+/26.5\right)\right]^2$, and the coefficient C_μ equal to 0.09. To incorporate drag reduction effects upon the turbulent viscosity the damping function $f_{DR}{}^p$ and the coefficient $C_\mu{}^P$ were introduced,

$$\nu_T = C_\mu \times f_\mu \times \frac{k^2}{\tilde{\varepsilon}^N}\left(1 - C_\mu{}^P \times f_{DR}{}^P \times \left(\frac{C_{mm}}{L^2}\right)^{0.25}\right) \tag{9}$$

with $f_{DR}{}^P = \left[1-\exp\left(-We_{\tau 0}/6.25\right)\right]^4$ and $C_\mu{}^P = 0.962$.

The main purpose of the extra polymeric turbulent viscosity, shown in Eq. (6), is to correct the balance of energy especially in the production term, P_k, next to the wall. The closure was developed following the ideas of Iaccarino et al. [7], and is given by

$$\nu_T{}^{p*} = 0.8\left(\frac{25}{We_{\tau 0}}\right)\frac{\lambda k}{C_{mm}} \tag{10}$$

Without the extra polymeric turbulent viscosity the turbulent kinetic energy (k) would vary in inverse proportion to the drag reduction as in previous models [6, 8] and in contrast to the correct behavior [9, 10]. The inclusion of this new quantity makes turbulent kinetic energy to increase with DR, as it should. Figure 1 compares the prediction (solid lines) of the production of k, P_k, with the results of DNS simulations (symbols) at DR=18% and 37%, corresponding to low and intermediate DR, respectively. The new model clearly improves on the predictions of the previous model, also included as dashed lines, especially close to the wall (y^+<20). The peak value of P_k is predicted to within 10% and its location is also well predicted, for both drag reductions.

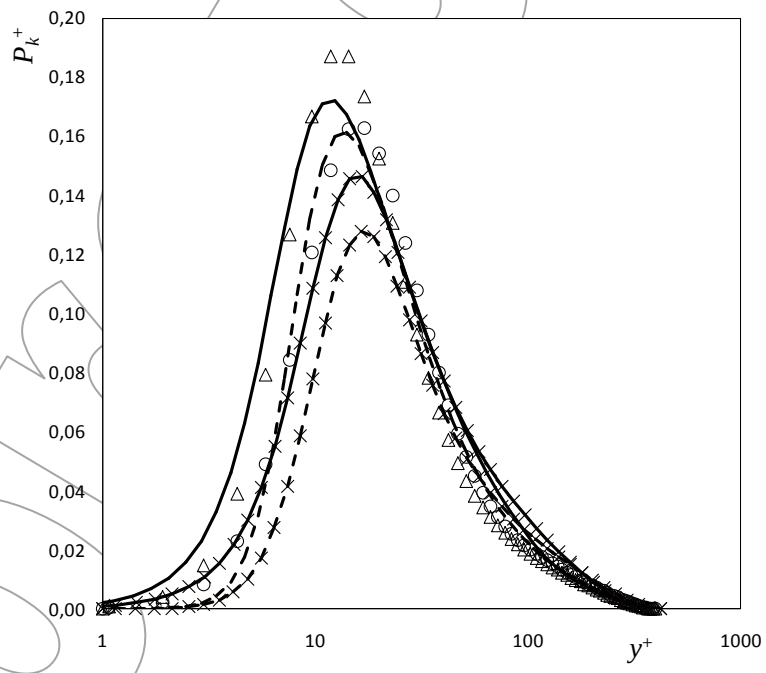

Figure 1: Comparison between DNS data (symbol: Δ DR=18%; ○ DR=37%) and predictions of the production term, P_k, with (continuum lines: — DR=18%; ⋆ DR=37%) and without (dash lines: — — DR=18%; —×— DR=37%) the extra polymeric turbulent viscosity, Eq. (10).

The closure for the Reynolds stress tensor requires the two remaining transport equations, one for the turbulent kinetic energy and the other for its rate of dissipation given by Eqs. (11) and (12), respectively

$$\frac{\partial \rho k}{\partial t}+\frac{\partial \rho U_i k}{\partial x_i}=\frac{\partial}{\partial x_i}\left[\left(\eta_s+\frac{\rho f_T \nu_T}{\sigma_k}\right)\frac{\partial k}{\partial x_i}\right]+P_k-\rho\tilde{\varepsilon}^N-\rho D+Q^V-\rho\varepsilon^V \tag{11}$$

$$\frac{\partial \rho \tilde{\varepsilon}^N}{\partial t}+\frac{\partial \rho U_i \tilde{\varepsilon}^N}{\partial x_i}=\frac{\partial}{\partial x_i}\left[\left(\eta_s+\frac{\rho f_T \nu_T}{\sigma_\varepsilon}\right)\frac{\partial \tilde{\varepsilon}^N}{\partial x_i}\right]+f_1 C_{\varepsilon_1}\frac{\tilde{\varepsilon}^N}{k}P_k-f_2 C_{\varepsilon_2}\rho\frac{\tilde{\varepsilon}^{N^2}}{k}+\rho E+E_{\tau_p} \tag{12}$$

where the turbulence production is $P_k=-\rho\overline{u_i u_j}\partial U_i/\partial x_j$, and Q^V and ε^V are viscoelastic terms in the equation for *k* representing the viscoelastic turbulent transport (Eq. (13)) and the viscoelastic dissipation (Eq. (14)). The second transport equation is actually for the modified rate of dissipation, $\tilde{\varepsilon}^N$, which is related to the true rate of dissipation through $\varepsilon^N=\tilde{\varepsilon}^N+D$, where term *D* is given by Eq. (16), which also contains a viscoelastic contribution by $\nu_{\tau_p}=\tau_{12}{}^P/\left(\partial U/\partial y\right)$. The transport equation for the modified rate of dissipation includes also a viscoelastic destruction term denoted E_{τ_p} and modelled in Eq. (15)).

$$Q^V\equiv\frac{\partial\overline{\tau'_{ik,p}u_i}}{\partial x_k}\approx\frac{\eta_p}{\lambda}\frac{\partial}{\partial x_k}\left[f\left(C_{mm}\right)\left(\frac{C_{ik}FU_i+CU_{iik}}{2}\right)\right] \tag{13}$$

$$\varepsilon^V\equiv\frac{1}{\rho}\overline{\tau'_{ik,p}\frac{\partial u_i}{\partial x_k}}\approx 1.37\times f_{DR}{}^p\frac{\eta_p}{\rho\lambda}f(C_{mm})\frac{NLT_{mm}}{2} \tag{14}$$

$$E_{\tau_p}\approx -f_5\times f_{DR}\times\frac{\tilde{\varepsilon}^{N2}}{k}\left[C_{\varepsilon F1}\times\frac{\varepsilon^V}{\tilde{\varepsilon}^N}+C_{\varepsilon F2}\times\left(\frac{25}{We_{\tau 0}}\right)^{2.1}\times\left(\frac{C_{mm}\times f\left(C_{mm}\right)}{L^2-3}\right)^2\right] \tag{15}$$

$$D=2\left(\nu_s+\nu_{\tau p}\right)\left(\frac{d\sqrt{k}}{dy}\right)^2 \tag{16}$$

$$E=\nu_s\nu_T\left(1-f_\mu\right)\left(\frac{\partial^2 U_i}{\partial y\partial y}\right)^2 \tag{17}$$

$$CU_{ijk}=-C_{\beta 1}\sqrt{\frac{25}{We_{\tau 0}}}\frac{\lambda}{f\left(C_{mm}\right)}\left(\overline{u_i u_m}\frac{\partial C_{kj}}{\partial x_m}+\overline{u_j u_m}\frac{\partial C_{ik}}{\partial x_m}\right)-C_{\beta 2}\left(\frac{We_{\tau 0}}{25}\right)^{1.661}\left[\pm\sqrt{\overline{u_j^2}}C_{ik}\pm\sqrt{\overline{u_i^2}}C_{jk}\right] \tag{18}$$

$$C_{ik}FU_i=C_{FU}\sqrt{\frac{We_{\tau 0}}{25}}C_{kn}\frac{\partial\overline{u_i u_i}}{\partial x_n} \tag{19}$$

The trace of the NLT_{ij} tensor (NLT_{mm}) is calculated by its viscoelastic closure (Eq. (5)). The remaining coefficient values and damping functions used in the viscoelastic turbulent model are listed in Table 1.

Table 1: Parameters values and damping functions.

Parameters values				
$C_{F1}=0.8$	$C_{F2}=0.0091$	$C_{F3}=0.042$	$C_{F4}=1.1$	$C_{\varepsilon_F}=2$
$C_\mu=0.09$	$C_{\varepsilon_1}=1.45$	$C_{\varepsilon_2}=1.9$	$\sigma_k=1.1$	$\sigma_\varepsilon=1.3$
$C_{\beta 1}=0.6$	$C_{\beta 2}=0.05$	$C_{FU}=0.031$	$C_{\varepsilon F1}=1.6$	$C_{\varepsilon F2}=1.74$
Damping functions				
$f_T=1+3.5\exp\left(-\left(\mathrm{Re}_T/150\right)^2\right)$		$f_5=\left[1-\exp\left(-y^+/50\right)\right]$		
$f_1=1$		$f_2=1-0.3\exp\left(-\left(\mathrm{Re}_T\right)^2\right)$		
$f_{F1}=\left(1-0.8\exp\left(-y^+/30\right)\right)^2$		$f_{F2}=\left(1-\exp\left(-y^+/25\right)\right)^4$		

Note: The f_T damping function depends on the turbulent Reynolds number, $\mathrm{Re}_T = k^2/(\varepsilon \cdot \nu_s)$

3 RESULTS

The performance of the new viscoelastic turbulence model is analyzed here through comparisons with Reynolds-averaged DNS data for turbulent channel flow at the same Reynolds number, $Re_{\tau 0} = 395$, which is defined by $Re_{\tau 0} = h \cdot u_\tau / \nu_0$, based on channel half-height, *h*. Other relevant flow conditions are $\beta = 0.9$, the ratio between the solvent kinematic viscosity and the zero shear-rate kinematic viscosity of the fluid, $\beta = \nu_s / \nu_0$, $L^2 = 900$, and Weissenberg numbers of 25 and 100, equivalent to DR=18% and 37%, respectively.

The DNS and predicted velocity profiles are compared in Figure 2 for DR=18% and 37%, including also the predictions by the previous turbulence model. The new model is better than the previous model [6], but the direct impact of the extra polymeric turbulent viscosity of Eq. (10) upon the momentum equation is rather small because the numerical method used here imposes the drag reduction and computes the required mean velocity.

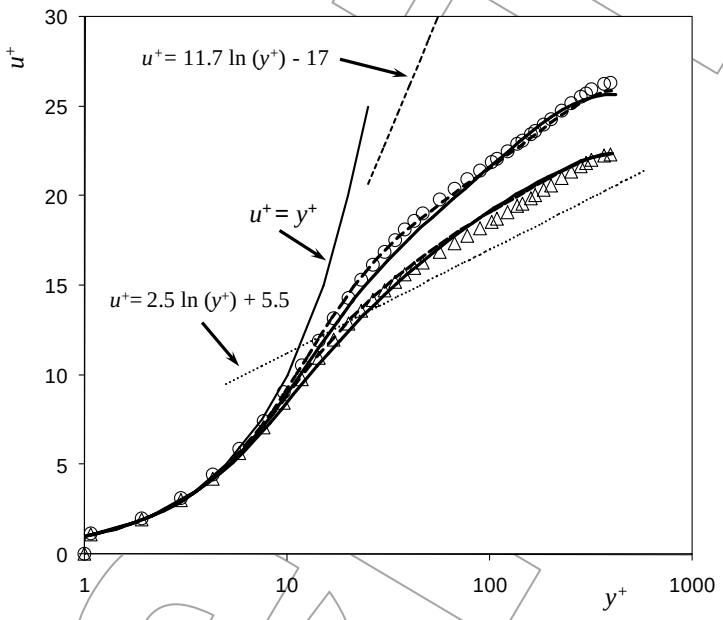

Figure 2: Comparison of the velocity profile between DNS data (symbol: Δ DR=18%; ○ DR=37%) and predictions: with the new model of the extra polymeric turbulent viscosity, Eq. (10), (continuum lines) and without (dash lines), [6].

The main effect of the new model of Eq. (10) is shown in Figure 3, which compares DNS data of the normalized turbulent kinetic energy with the old and new predictions. Whereas the previous closure under-predicted *k* by nearly 30%, the new model predictions are within 10% of the DNS data. The correction is restricted to a small region very close to the wall, but its impact on the profile of *k* is very large and allows the correct prediction of the Reynolds stress without the need to dampen the turbulent kinetic energy. This also allows the use of this full *k*-ε type model to the full range of drag reductions, contrasting with the limited range of the previous model to a value of DR of about 50%.

4 CONCLUSIONS

Previous RANS type turbulence models for FENE-P fluids showed a deficit of *k* very close to the wall and this was traced to a deficit in the production of *k*. In this work a modification is introduced in the closure for the Reynolds stress that corrects that deficiency and consequently the Reynolds shear stress in boundary layer flows becomes well predicted under intense drag reduction conditions without the need for an excessive damping of the turbulent kinetic energy as was the case in some past turbulence models [6]. The modification is the introduction of an extra polymeric contribution to the turbulent viscosity, which is based on the fluid relaxation time. This new contribution is restricted to the near-wall region.

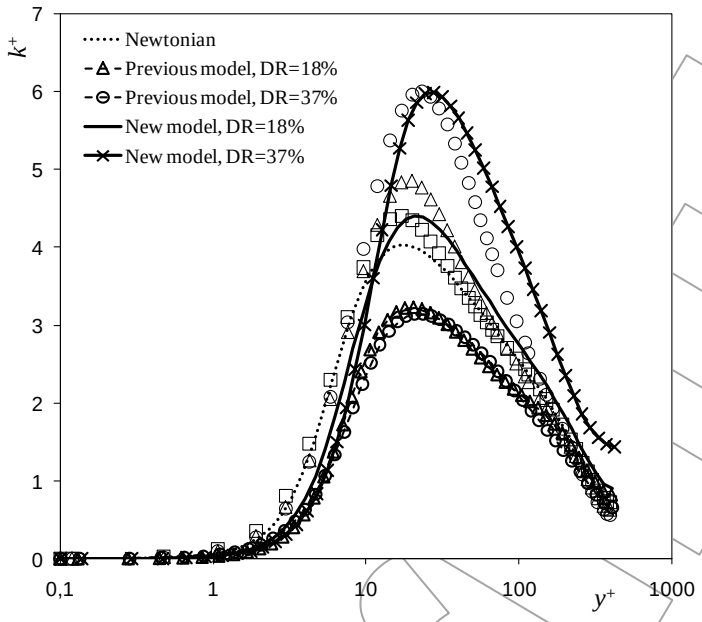

Figure 3: Comparison of turbulent kinetic energy between DNS data (symbols: □ Newtonian; Δ DR=18%; ○ DR=37%) and predictions with the model of the extra polymeric turbulent viscosity, Eq. (10) and without such model [6].

ACKNOWLEDGMENTS

Financial support provided by FAPESP - Fundação de Amparo à Pesquisa do Estado de São Paulo through Project Nº 2013/01521-4 and FUNDUNESP Process / EDITAL Nº: 1854/009/13 - PROPe / CDC is gratefully acknowledged by P. R. Resende.

REFERENCES

[1] R. Sureshkumar, A. N. Beris and R. A. Handler (1997). Direct numerical simulation of the turbulent channel flow of a polymer solution. *Physics of Fluids*, 9 (3), 743-755.

[2] C. D. Dimitropoulos, R. Sureshkumar, A. N. Beris and R. A. Handler (2001). Budgets of Reynolds stress, kinetic energy and streamwise entrophy in viscoelastic turbulent channel flow. *Physics of Fluids*, 13 (4), 1016-1027.

[3] C. F. Li, V. K. Gupta, R. Sureshkmar and B. Khomami (2006). Turbulent channel flow of dilute polymeric solutions: drag reduction scaling and an eddy viscosity model. *Journal of Non-Newtonian Fluid Mechanics*, 139, 177-189.

[4] K. Kim, C. F. Li, R. Sureshkumar, S. Balachandar and R. Adrian (2007). Effects of polymer stresses on eddy structures in drag-reduced turbulent channel flow. *Journal of Fluid Mechanics*, 584, 281-299.

[5] F. T. Pinho, C. F. Li, B. A. Younis and R. Sureshkumar (2008). A low Reynolds number k-ε turbulence model for FENE-P viscoelastic fluids. *Journal of Non-Newtonian Fluid Mechanics*, 154, 89-108.

[6] P. R. Resende, K. Kim, B. A. Younis, R. Sureshkumar and F. T. Pinho (2011). A FENE-P k–ε turbulence model for low and intermediate regimes of polymer-induced drag reduction. *Journal of Non-Newtonian Fluid Mechanics*, 166 (12-13), 639–660.

[7] Gianluca Iaccarino, Eric S.G. Shaqfeh and Yves Dubief (2010). Reynolds-averaged modeling of polymer drag reduction in turbulent flows. *Journal of Non-Newtonian Fluid Mechanics*, 165 (7-8), 376–384.

[8] P. R. Resende, F. T. Pinho, K. Kim, B. A. Younis and R. Sureshkumar (2013). Development of a Low-Reynolds-number k-ω Model for FENE-P Fluids. *Flow, Turbulence and Combustion*, 90 (1), 69-94.

[9] K. D. Housiadas and A. N. Beris (2003). Polymer-induced drag reduction: Effects of the variations in elasticity and inertia in turbulent viscoelastic channel flow. *Physics of Fluids*, 15 (8), 2369-2384.

[10] C. F. Li, R. Sureshkmar and B. Khomami (2006). Influence of rheological parameters on polymer induced turbulent drag reduction. *Journal of Non-Newtonian Fluid Mechanics*, 140, 23-40.